THE JOURNAL OF PHYSICAL CHEMISTRY B

Article

pubs.acs.org/JPCB

Cholesterol Modulates the Structure, Binding Modes, and Energetics of Caveolin–Membrane Interactions

Durba Sengupta*

National Chemical Laboratory, Council of Scientific and Industrial Research, Dr. Homi Bhabha Road, Pune 411008, India

Supporting Information

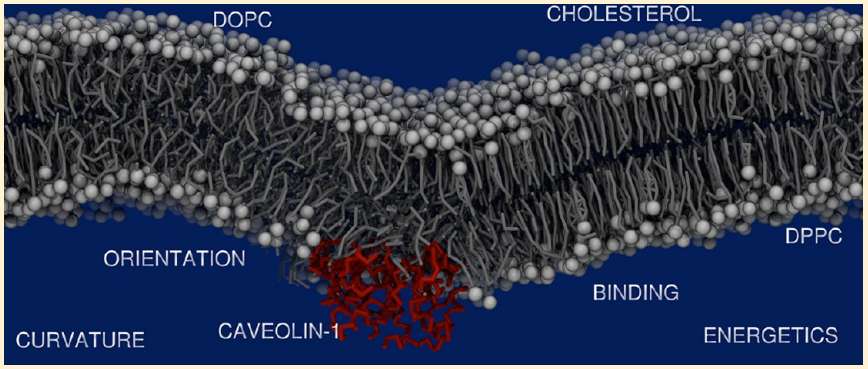

ABSTRACT: Caveolin-1 (cav-1) is an important membrane protein that plays a vital role in cellular signaling and trafficking by organizing membrane domains. The peptide interacts with cholesterol-rich membranes and induces large morphological changes in them, forming microdomains such as caveolae. Here, we use coarse-grain molecular dynamics simulations to study the interaction of cav-1 peptides with several model bilayer systems mimicking biological scenarios, such as cholesterol-rich domains, cholesterol-depleted domains, and unsaturated lipid domains. We show that cholesterol modulates the depth as well as orientation of cav-1 binding to membranes. Furthermore, the presence of cholesterol stabilizes more open conformations of cav-1, and we speculate that the binding modes and open conformations could be responsible for inducing morphological changes in the bilayer. We also calculated the partitioning free energy to different bilayers and show that binding to cholesterol-rich bilayers is more favorable than cholesterol-depleted bilayers and the binding to unsaturated bilayers is the least favorable. Binding to cholesterol-rich bilayers also changes the pressure profile of the bilayer to which it is bound and thereby affects the local spontaneous curvature. Our results highlight molecular details of protein–lipid interplay and provide new insights into the effects of cav-1 in tuning the morphology of cholesterol-rich membranes.

INTRODUCTION

Caveolin-1 (cav-1) is the most common member of the caveolin family and plays multiple roles in cellular signaling, lipid exchange, endocytosis, and intracellular delivery of bacterial toxins.[1−3] Misregulation and mutations of cav-1 have been implicated in a variety of diseases including cancer and neurodegeneration.[4−6] Interactions of cav-1 with cholesterol-rich membranes result in changes in membrane morphology and the eventual formation of 50−100 nm invaginations known as caveolae, that have multiple roles in signal transduction, especially in endocytosis. Smaller nanodomains known as "cav-1 scaffold" that could induce local changes in membrane topology and composition have also been reported and shown to be distinct from caveolae.[2] Within the cav-1 scaffolds, cav-1 acts as a scaffolding protein by compartmentalizing and concentrating signaling molecules, such as receptor tyrosine kinases.[7,8]

Consistent with its role in organizing caveolar domains or cav-1 scaffolds, cav-1 has been shown to insert into membranes in a cholesterol-dependent manner.[9,10] Upon membrane interaction, it is thought to be anchored to the membrane *via* a hydrophobic central region as well as with three palmitoyl chains attached to cysteine residues at the C-terminal region.[9,11,12] A mutant form of caveolin with the three palmitoylation sites removed still translocates to caveolae, thus suggesting that the central region is responsible for the increased interaction with cholesterol-rich domains and targeting the full-length protein to caveolae.[10,11]

NMR and CD studies have revealed that the central intramembrane region of cav-1, spanning residues 102−122, forms a central helical hairpin structure.[13−15] It has been proposed that the bent helix structure of the intramembrane region is directly related to its function.[16] The intramembrane region is thought to be inserted into the membrane without completely traversing it, thus forming a re-entrant helix.[14,16] A single point mutation, P110A, has been shown to change the

Received: August 6, 2012
Revised: November 29, 2012
Published: November 30, 2012

structural characteristics of this re-entrant helix and affect its membrane binding and partitioning.[12] The ability of the mutant to form caveolae-like structures is also distinctly reduced,[12] pointing to a relation between the mode of binding and function. It has been suggested by recent fluorescence experiments that the intramembrane region of cav-1 inserts less deep in the presence of cholesterol,[16] contradicting an earlier report.[17] However, the exact mode of binding of this region such as the depth and orientation of insertion, and whether cholesterol plays a role in modulating its membrane binding is not known.

The cytoplasmic N- and C-terminal domain lying at either side of the central hairpin structure are more unstructured with varying degrees of helical and β-strand character.[13,14] The N-terminal residues comprise the oligomerization domain (residues 60−90)[10] and the caveolin scaffolding domain containing the putative cholesterol binding CRAC motif (residues 94−101).[17] However, fragments of the caveolin scaffolding domain all containing the CRAC motif but of varying lengths showed variable tendencies toward promotion of cholesterol-rich domains.[17] In fact, the authors suggest that the CRAC motif may not be directly involved in cholesterol binding, since such an interaction would inhibit formation of cholesterol crystals or domains by stabilizing the cholesterol that is bound to the peptide.[17] The C-terminal domain of cav-1 has been reported to promote protein−protein interactions as well as membrane attachment.[10] It contains three palmitoylated cysteines[11] that were shown to be not essential for either membrane anchorage or caveolae localization, though they appear to be critical for other functions such as the transportation of cholesterol.[18] However, the molecular and structural details of cav-1−membrane interactions and how they vary in a cholesterol-dependent manner are still unclear.

In analyzing the molecular level details of membrane-related processes, state-of-art molecular dynamics simulations have managed to fill the gap left by experimental studies that arise due to the technical challenges and inherent resolution limits existing in biophysical experimental techniques (see Reviews[19,20]). Simulations of membrane-active peptides such as antimicrobial peptides,[21−23] cell penetrating peptides,[24,25] and fusion peptides[26−28] have revealed several aspects of their function. The understanding of the molecular basis of curvature generation by peptides during vesicle budding events is much more limited, and only peptides containing the BAR and N-BAR domains[29,30] have been studied. Computer simulations have shown that the proteins containing the BAR domains create curvature by acting as a scaffold, forcing the membrane to locally adopt its intrinsic shape.[30] It remains however unclear how peptides such as cav-1 that have a much shorter membrane binding domain and do not have the characteristic "banana shape" interact with membranes in a composition-dependent manner and how these binding modes lead to changes in membrane topology.

Here, we carry out molecular dynamics simulations using the coarse-grain MARTINI force-field to analyze association of cav-1 with cholesterol-rich and cholesterol-depleted bilayers. The MARTINI force-field is used, since it has been shown to be able to successfully explain membrane binding,[31,32] partitioning between different membrane phases,[33] and membrane topology changes.[26,28,34] We focus on the intramembrane and caveolin scaffolding domains to extract out the functionally relevant differences in binding and topology between cholesterol-rich and cholesterol-depleted bilayers. We compare the structural properties of cav-1 as well as the binding modes in the presence and absence of cholesterol and speculate whether the differences seen in the simulations could be responsible for inducing morphological changes in the bilayer. To understand the origin of the morphological changes, we have also calculated the stress profiles of the bilayers with bound peptide. Our results highlight the molecular details of cav-1−membrane interactions and provide an understanding of the effects of the peptide tuning the morphology of cholesterol-rich membranes.

METHODS

Simulation Setup. Coarse-grain molecular dynamics simulations were performed with the MARTINI force-field[35,36] to study the association of cav-1 with five model bilayer systems. The lipid bilayers that were studied were comprised of POPC (palmitoyloleoylphosphatidylcholine), POPC with 30% cholesterol, DPPC (dipalmitoylphosphatidylcholine), DPPC with 30% cholesterol, and DOPC (dioleoylphosphatidylcholine). The lipids were chosen to represent fully saturated lipids (DPPC), hybrid saturated−unsaturated lipids (POPC), fully unsaturated lipids (DOPC), and cholesterol enriched membranes (DPPC and POPC cholesterol mixed bilayer). Membranes of DPPC and DPPC with 30% cholesterol were simulated both below the transition temperature of DPPC (300 K) and above it (325 K) to study both gel-phase and fluid-phase behavior.

The peptide fragment containing residues 94−122 (VTKYWFYRLL SALFGIPMAL IWGIYFAIL) of the peptide that is comprised of the intramembrane and caveolin scaffolding domains was studied. The peptide was modeled as a helix−coil−helix based on NMR and CD data[13−15] using an in-house script and standard MARTINI parameters. The secondary structure of the peptide was maintained by adding dihedral potentials to the backbone atoms of the two helical stretches. (Please note that the tertiary structure of the peptide was not constrained by harmonic potentials or an elastic network.) The peptide structure was first equilibrated in a vacuum followed by equilibration in the water phase. The final representative conformation was used in the membrane systems.

The final simulation box consisted of a single copy of the cav-1 peptide that was placed in the water phase, at a distance of at least 4 nm from a pre-equilibrated bilayer. The system contained on average 300 lipids (or 220 lipids and 80 cholesterol) molecules and 7000 water beads. For simulations carried out at 300 K, antifreeze particles were added to keep the water in the fluid phase, as is common with the MARTINI force-field.[35] Simulations of the peptide in a water box were also performed for comparisons. Simulations were carried out for 40 μs for each system.

Simulation Protocol. The MARTINI force-field[35,36] was used to describe the peptide, lipids, and water. The molecular dynamics simulations were performed using the GROMACS program package,[37] with the scheme developed for coarse-grain simulations, under periodic boundary conditions. The temperature was weakly coupled (coupling time 0.1 ps) to a thermostat at 300 or 325 K using a Berendsen algorithm.[38] The pressure was also weakly coupled (coupling time 1.0 ps, compressibility 5×10^{-5} bar^{-1}) using a semi-isotropic coupling scheme, in which the lateral and perpendicular pressures are coupled independently at 1 bar.[38] The nonbonded interactions were treated with a switch function from 0.0 to 1.2 nm for the Coulomb interactions and 0.9 to 1.2 nm for the LJ interactions

dx.doi.org/10.1021/jp3077886 | J. Phys. Chem. B 2012, 116, 14556−14564

(pair-list update frequency of once per 10 steps). A time step of 20 fs was used. The simulation times reported in the manuscript are actual simulation times (which multiplied by a factor of 4 gives the effective times).[35,36]

Analysis. *Depth of Binding.* The depth of insertion of the peptide was calculated as the difference of the position (along the z axis) of the center of mass of the peptide and the average position of the phosphate bead of the leaflet to which it is bound. The depth of insertion of the two tryptophan residues (Trp 98 and Trp 115) was calculated accordingly. The maximum insertion was calculated as the depth of binding of the deepest peptide bead at each time point. Only the last 30 μs was considered for analysis.

Orientation. The orientation of the helices was calculated as the angle formed by the helical axis and the z-axis. The helix axis was defined as the axis joining the backbone atoms of residues 4 and 11 in helix 1 and 22 and 26 in helix 2. This simple method does not accurately describe the helix axis but is adequate for calculating and comparing the changes in the orientation of the helices, especially in the presence of secondary structural constraints. Only the last 30 μs was considered for analysis.

Interhelical Angle. The interhelical angle was calculated as the angle between the two helix axes, as defined above. Only the last 30 μs was considered for analysis.

Radius of Gyration. The radius of gyration was calculated for the last 30 μs of simulation using the GROMACS tool.

Free Energy Calculations. The partitioning free energy of a peptide between water and the membrane phase, $\Delta G_{\text{water/membrane}}$, was determined as the difference between the solvation free energies in water and the membrane environment. The solvation free energy, i.e., the free energy of extracting a peptide from the membrane (or water) to the gas phase, was determined by thermodynamic integration (TI) with a coupling parameter λ similar to the protocol described in ref 33. This was done in two steps: First, all nonbonded interactions of the peptide with the surrounding bilayer and water as well as within the peptide were turned off; second, the interactions were turned back on in vacuo, wherein $\lambda = 0$ and $\lambda = 1$ correspond to the fully coupled and uncoupled states, respectively. The helicity of the cav-1 peptides is imposed by the dihedral (bonded) interactions, and is thus not affected during the TI. The distance between the center of mass of the peptide and the center of the bilayer was kept close to the value calculated from the previous simulations (spontaneous binding of the peptide to the lipid bilayer) by means of a harmonic position restraint along the bilayer normal (force constant 1000 kJ mol^{-1} nm^{-2}). This restraint prevents the peptide from slipping out of the bilayer at λ close to 1, while still allowing it to diffuse, and reorient in the bilayer. A soft-core potential was used for the nonbonded Lennard-Jones interactions with potential height $\alpha = 1.3$, λ-power = 1, and interaction range $\sigma =$ 0.47 nm. We used a basic spacing between the λ-points of 0.05, yielding a total of 21 λ-points. At each λ-point, the system was simulated for 1 μs (which, using the time conversion factor of 4 observed for simple bilayer systems, corresponds to about 4 μs of atomistic simulation time).

Lipid Chain Order Parameters. The second-rank order parameter, $P_2 = 1/2(3\langle\cos^2\theta - 1\rangle)$, was computed for consecutive bonds in the CG lipids, with θ being the angle between the bond vector and the bilayer normal. The broken brackets denote an ensemble average. Perfect alignment with the bilayer normal is indicated by P2 = 1, perfect antialignment by P2 = −0.5, and a random orientation by P2 = 0. Order parameters were calculated by averaging over the last 30 μs of the trajectory.

Pressure Profile. For a system with planar symmetry such as a lipid bilayer, the local pressure can be divided into planar $P_L = (P_{xx} + P_{yy})/2$ and normal (along the membrane normal direction) $P_N = P_{zz}$ components. The lateral pressure profile $p(z)$ is then defined as a difference between the normal and the lateral components of the pressure tensor, that is, $p(z) = P_L - P_N$. The lateral pressure profiles were calculated as described in ref 39 after removal of the center of mass motion of the peptide. The lateral pressure profiles were calculated for the entire bilayer as well as a smaller patch of 4 nm from the peptide.

Simulations of the pure bilayer systems were also performed for comparisons. Simulations were carried out for 1 μs for each system corresponding to an effective simulation time of 4 μs.

Spontaneous Curvature. The spontaneous monolayer curvature c_0 was calculated from the first moment of the stress:

$$c_0 = \frac{1}{k_m}\int_0^\infty zp(z)\,dz$$

where k_m is the monolayer bending modulus and equal to half the bilayer bending modulus ($k_b/2$) and z is the distance across the membrane relative to the center of the bilayer ($z = 0$). Since the expression is not independent of the choice of definition of local pressure, it should be used as a qualitative measure. Positive values for the radius of spontaneous curvature reflect an increased preference for positively curved surfaces (such as in micelles and pores), and increasingly negative values correspond to an increasing preference for negatively curved surfaces (such as in stalks and inverted hexagonal phase).

RESULTS AND DISCUSSION

To study the interaction of cav-1 with biomembranes, the membrane binding fragment of the peptide (VTKYWFYRLL SALFGIPMAL IWGIYFAIL) was simulated with five model bilayers—DPPC, DPPC with 30% cholesterol, POPC, POPC with 30% cholesterol, and DOPC. The lipids were chosen to represent cholesterol-enriched membranes (DPPC−cholesterol and POPC−cholesterol mixed bilayers) that cav-1 peptides have been shown to have increased interactions with, the corresponding pure bilayers (DPPC and POPC), and a fully unsaturated lipid (DOPC) that is believed to be excluded from the more ordered caveolin domains. Membranes of DPPC and DPPC with 30% cholesterol were simulated both below the transition temperature of DPPC (300 K) and above it (325 K) to study both gel-phase and fluid-phase behavior.

In all the simulations, the peptide diffused at a nanosecond time scale to the membrane and became bound to it. After binding, the peptide was present at the interface and interacted mainly with the headgroup region. A snapshot of the peptide bound to two representative membranes, DPPC and DPPC−cholesterol bilayers, is shown in Figure 1. To understand the underlying molecular driving forces for the interaction of cav-1 peptides with the different bilayers, we analyzed its binding mode, structural properties, and partitioning energies.

Cholesterol Modulates the Depth of Insertion of Cav-1. Cav-1 peptides bind at the membrane−water interface and penetrate to different depths in the five bilayer systems simulated. The depths of insertion reach equilibrium values at a nanosecond time scale and are surprisingly stable even at a

dx.doi.org/10.1021/jp3077886 | J. Phys. Chem. B 2012, 116, 14556−14564

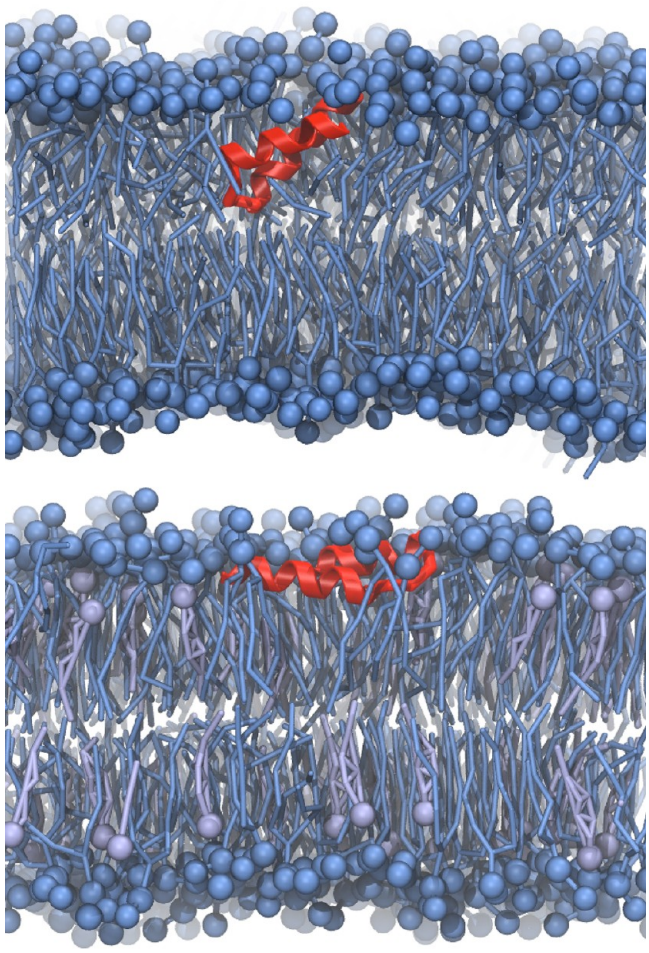

Figure 1. Snapshot of cav-1 peptides bound to DPPC (top) and DPPC−cholesterol (bottom) bilayers. The peptide is represented in red, the DPPC molecules in blue, and the cholesterol molecules in violet. The water molecules present in the simulations are not represented for clarity.

microsecond time scale. Figure 2 shows the depth of insertion of the peptide (center of the mass) for the two systems

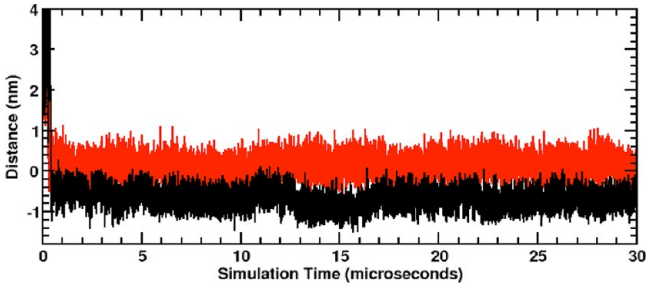

Figure 2. Time course of the insertion of the cav-1 peptide in DPPC (black) and DPPC−cholesterol (red) bilayers. The values of insertion are calculated as the difference in the position of the center of mass of the peptide and the phosphate beads of the leaflet to which it is bound.

represented in Figure 1: DPPC and DPPC−cholesterol mixed bilayers. The average depth of insertion of the center of mass (COM) of the peptide, the tryptophan residues (Trp 98 and 115), and the maximum depth of insertion was also calculated and is shown in Figure 3A (see also Table 1). The tryptophan insertion has been calculated to be able to compare to

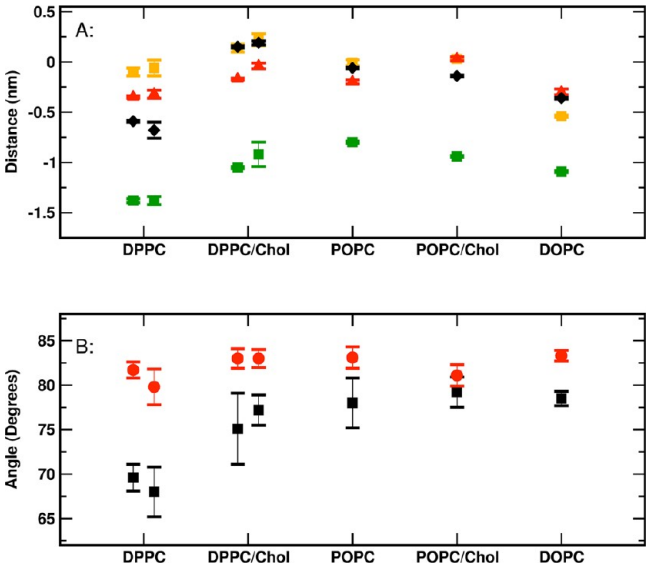

Figure 3. Binding of cav-1 to model bilayers. Top: The depth of binding of cav-1 to the five model membranes w.r.t. the phosphate beads of the leaflet to which it is bound. The value of the insertion of center of mass of the peptide is shown in black, the maximum insertion in green, and the insertion of the tryptophan residues in red and orange. Bottom: The orientation of helix 1 (black) and helix 2 (red) of cav-1 w.r.t. to the bilayer normal. For DPPC and DPPC−cholesterol membranes, the values calculated at 300 K are plotted first (left) followed by the values at 325 K (right).

experimental data on the change in the tryptophan fluorescence upon membrane binding. A comparison of the values of the depth of binding reveals that the peptide inserts the most in pure DPPC bilayers and the least in DPPC−cholesterol mixed bilayers. Insertion in POPC and DOPC as well as POPC−cholesterol mixed bilayers is similar and is in between that of DPPC and DPPC−cholesterol bilayers. Interestingly, the insertion of the peptide (both COM and maximum insertion) is greater in pure DPPC bilayers compared to DPPC−cholesterol but is marginally less in POPC compared to POPC−cholesterol bilayers. When we consider the depth of binding of the tryptophan residues (Trp 98 and Trp 115) a larger flexibility is seen in the data. The binding of the two tryptophan residues does not always reflect the trends in the COM binding depth, nor do they always show the same trend individually.

The depths of insertion calculated in our simulations appear to explain seemingly contradictory results that indicated an increased[16] as well as a marginal decrease[17] in the insertion of cav-1 peptides in the absence of cholesterol. In the study of Aoki et al.,[16] they concluded that the peptide binds deeper in the absence of cholesterol based on the change of tryptophan fluorescence in mixed bilayers of cholesterol, DPPC and POPC. In their previous study,[17] however, they had used only POPC and POPC cholesterol bilayers and had reported a marginal decrease in depth of binding in the presence of cholesterol based on NMR as well as fluorescence data. This can be correlated to the significantly deeper binding of the peptide observed in our simulations in the absence of cholesterol in DPPC−cholesterol mixed bilayers but not in POPC−cholesterol mixed bilayers. By comparing experimental data to simulation results, we see that the trends in the binding depths of tryptophan residues do not always reflect the actual insertion

dx.doi.org/10.1021/jp3077886 | J. Phys. Chem. B 2012, 116, 14556−14564

Table 1. The Binding Modes and Energetics of cav-1−Membrane Interactions[a]

property	DPPC	DPPC−Chol	POPC	POPC−Chol	DOPC
insertion (nm)	−0.59 ± 0.01	+0.15 ± 0.01	−0.06 ± 0.01	−0.14 ± 0.01	−0.36 ± 0.01
	−0.68 ± 0.08	+0.19 ± 0.02			
orientation (deg)	69.6 ± 1.5	75.1 ± 3.9	78.0 ± 2.8	79.2 ± 1.8	78.5 ± 0.8
	68.0 ± 2.8	77.2 ± 1.7			
free energy (kJ/mol)	−419.9 ± 12.4	−518.2 ± 7.6	−401.1 ± 3.5	−540.0 ± 12.6	−340.8 ± 14.1
	−322.4 ± 5.3	−338.0 ± 14.0			

[a]The depth of insertion of the peptide is defined as the difference of the center of mass of the peptide and the average position of the phosphate bead of the membrane leaflet to which it is bound. The orientation is calculated as the angle (in degrees) between helix 1 and the z axis. The free energies reported are the membrane/water partitioning free energies calculated via thermodynamic integration. The first row reports the values at 300 K and the second row at 325 K.

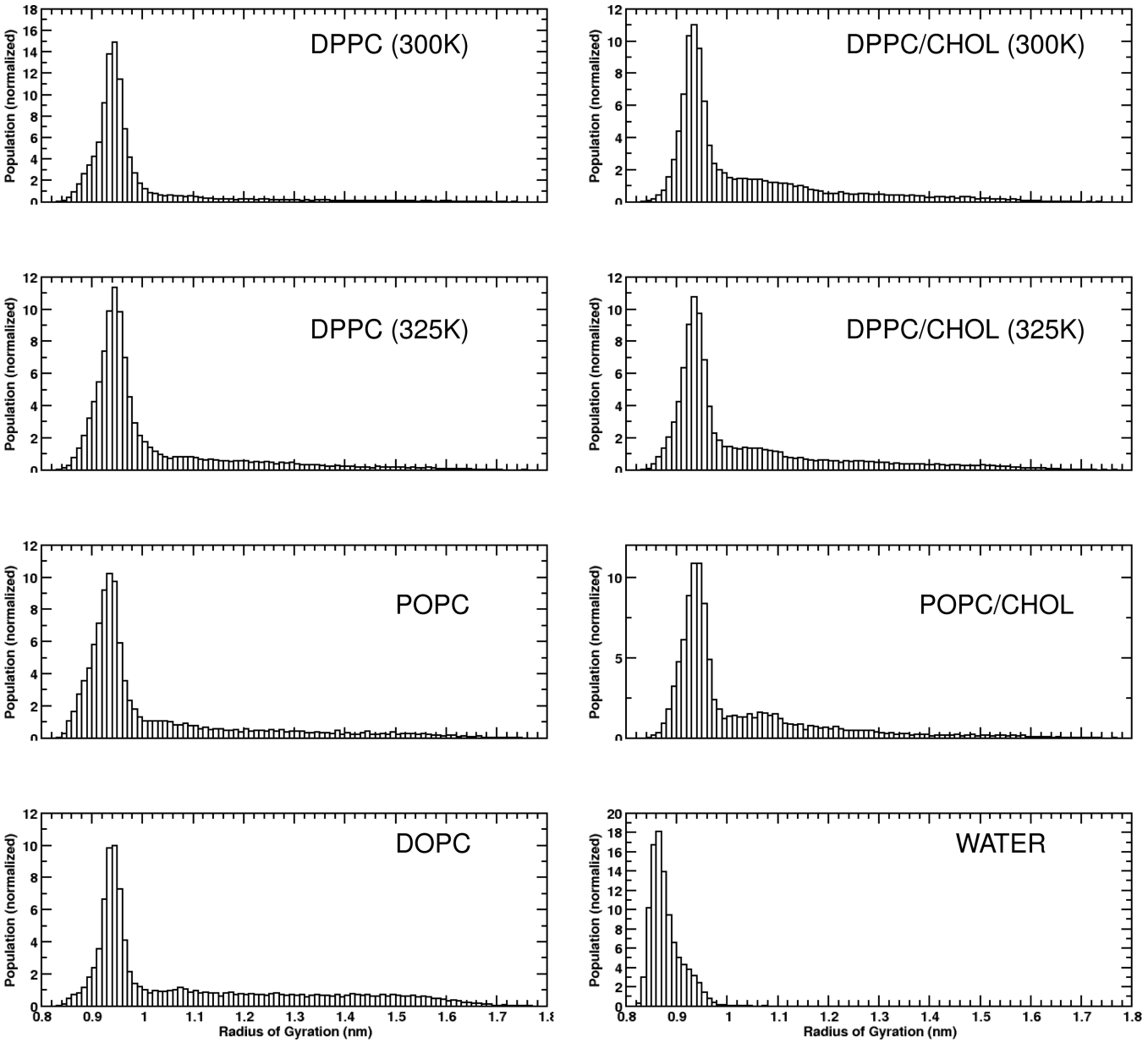

Figure 4. The population histograms of the radius of gyration of the cav-1 peptide sampled during the simulations in water and five bilayer systems.

of the peptide and, thus, comparisons to experimental data should be done with care.

Cav-1 Orients Parallel to the Bilayer Surface. After binding to the membrane, the peptide adopts an orientation parallel to the bilayer surface with the angle between the bilayer normal and the peptide close to 90°. During the time course of the simulation, the peptide orientation fluctuates around this value. Table 1 and Figure 3 show the angle between the bilayer normal and helix 1 and helix 2 of the peptide. Helix 1 adopts a more tilted orientation and orients at about 80° to the bilayer

dx.doi.org/10.1021/jp3077886 | J. Phys. Chem. B 2012, 116, 14556−14564

normal, i.e., about 10° to the bilayer surface. In DPPC, the helix tilts further and is oriented at an angle of about 15° to the bilayer surface. Helix 2 is less tilted in comparison to helix 1, but again in DPPC, the tilt is higher than in the other bilayers. A visual comparison between the representative binding modes of the peptides in DPPC and DPPC−cholesterol bilayers is shown in Figure 1. It is clearly seen that the peptide adopts a more inserted orientation in DPPC bilayers, while it is more surface-aligned in DPPC−cholesterol mixed bilayers.

Cholesterol Stabilizes Open Conformations of Cav-1. We also analyzed the radius of gyration of the peptide to analyze the compactness of the peptide conformation. Histograms showing the radius of gyration for all the simulations are shown in Figure 4. In water, the peptide adopts a very compact structure and the radius of gyration remains below 1 nm. This corresponds to the compact helical hairpin conformation. Upon interaction with the lipid bilayer, more open conformations were sampled. The peak of the distribution shifts to the right and a longer tailed distribution was seen, indicating that more "open" structures were also sampled. In the presence of cholesterol, a smaller second peak was seen between 1 and 1.1 nm. The increase in the population of open structures, though comprising only a fraction of the population, was seen consistently in all cholesterol-containing simulations compared to the same system when cholesterol was absent. In conclusion, it appears that cav-1 adopts a very compact structure in water, but upon membrane binding, more open conformations are sampled that are stabilized further in the presence of cholesterol.

One of the largest factors that contributes to the increased radius of gyration is the interhelical angle, i.e., the angle between the two helices of the helical hairpin structure. During the simulations, the peptide undergoes a breathing motion and the angle between the two helices fluctuates. We would like to point out here that the hairpin structure seen in cav-1 is stabilized only by Lennard-Jones interactions between the atoms of the two helices and no harmonic potential was present to keep the peptide in the hairpin structure (as done under the elastic network model[40] of the MARTINI force-field). The angle between the two helices is plotted in Figure 5 for DPPC and DPPC−cholesterol simulations along with the corresponding radius of gyration values. For both DPPC and DPPC−cholesterol membranes, the largest population of conformations has an interhelical angle of 30°, corresponding to the "compact" helical-hairpin structure. Conformations with much larger interhelical angles are also sampled but with a much lower population. In the presence of cholesterol, the population of structures with larger interhelical angles is increased. Though we cannot rule out the importance of the terminal residues in modulating the compactness of the helical hairpin structure, it appears that the population of more "open" structures increases in the presence of cholesterol.

No Preferential Binding of Cholesterol to CRAC Sites. In order to analyze the cholesterol binding at the CRAC sites, we calculated the cholesterol density around the peptide (Figure 6). The residues that comprise the CRAC motif, VTKYWFYR, are present toward the N-terminal of the intramembrane fragment and are labeled for reference. The density of cholesterol is the highest at the C-terminal and turn regions, and not in proximity to the CRAC residues. An increased density of cholesterol is seen around R101 and W98 of the CRAC motif compared to the bulk but is much lower than the density at the C-terminus and turn regions. We could thus not discern any preferential cholesterol binding at the putative cholesterol binding CRAC sites present at the N-terminus. However, we cannot rule out the importance of the deleted residues in modulating cholesterol binding at the CRAC sites.

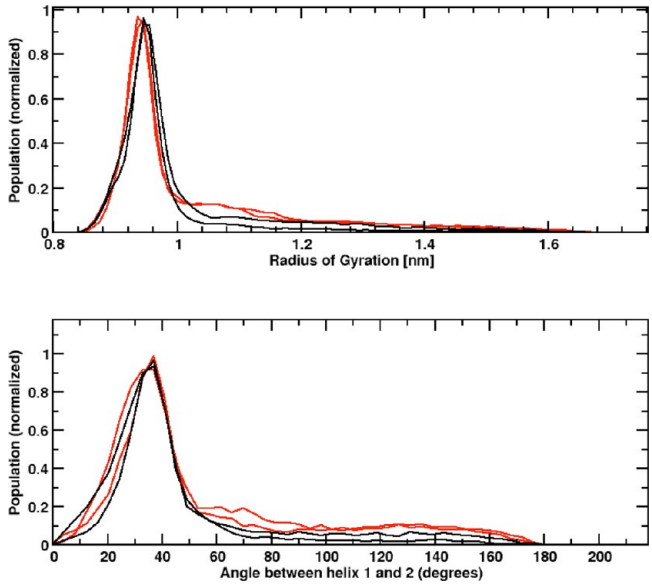

Figure 5. The population profiles of the radius of gyration (top) and interhelical angle (bottom) of the cav-1 peptide sampled during the simulations. The values for DPPC−cholesterol bilayers are plotted in red and DPPC bilayers in black.

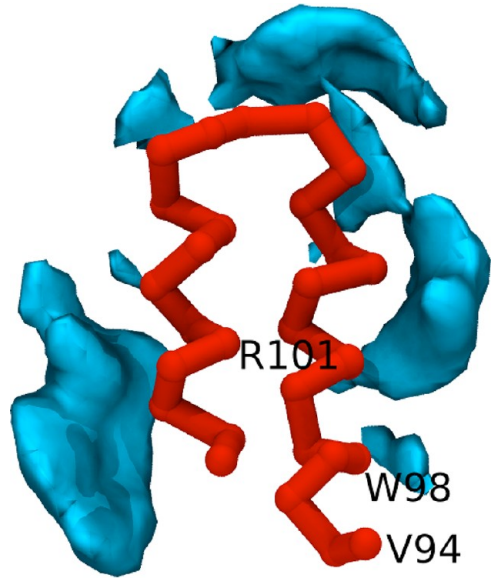

Figure 6. A representative snapshot of cav-1 peptide superimposed with the time-averaged density of cholesterol molecules. The residues V94, W98, and R101 that are a part of the CRAC motif are labeled for reference.

Cav-1 Binds Strongly to Cholesterol-Rich Bilayers. To understand the energetics and driving forces for the interaction of cav-1 peptides with the different bilayers, we calculated the partitioning free energies of a cav-1 peptide between water and membrane by thermodynamic integration. The results are summarized in Figure 7 and Table 1. The water/membrane partitioning energies were calculated as the difference of the

dx.doi.org/10.1021/jp3077886 | J. Phys. Chem. B 2012, 116, 14556−14564

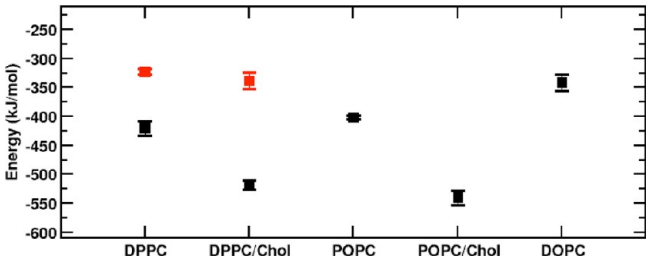

Figure 7. The partitioning free energy, $\Delta G_{water/membrane}$, between water and membrane for cav-1 peptide for the five model membrane systems. The values in black have been calculated at a temperature of 300 K, and the values in red are at 325 K.

solvation energies in water and membrane. The solvation free energy, ΔG_{solv}^{water}, is calculated to be 562.7 ± 15.4. For all the bilayers studied, a large negative partitioning energy, between water and the membrane, was obtained. Thus, the partitioning of cav-1 peptides on the membrane surface from the water is energetically favorable. We would like to note that the water/membrane partitioning energies of the individual amino acid residues have been calculated with the MARTINI force-field and are consistent with those calculated from atomistic simulations.[32] Furthermore, though the absolute magnitudes of partitioning energies differ from those of experimental scales calculated from model bilayers as well as biological membranes, the relative values are consistent.[32,41]

Among the five bilayer systems studied, a strong preference toward cholesterol-rich membranes is seen compared to pure lipid bilayers of the same composition. The most favorable binding free energy calculated is for cholesterol-rich bilayers. The difference in the free energy of partitioning between pure POPC bilayers and POPC−cholesterol mixed bilayers is ≈140 kJ/mol, consistent with the cholesterol-dependent partitioning seen for cav-1 peptides in bilayers.[9,10] For DPPC and DPPC−cholesterol bilayers, the difference between free energy of partitioning between the two systems is also very high, ≈100 kJ/mol. Interestingly, the free energy of partitioning to both pure DPPC as well as DPPC−cholesterol bilayers was reduced at higher temperatures when DPPC is in the fluid phase. The binding of cav-1 to DOPC bilayers appears to be the least favorable among the membrane compositions studied. This is not surprising, since unsaturated lipids, such as DOPC, are thought to be excluded from the more ordered cav1-rich caveolin domains. Altogether, it appears that, though the peptide binds strongly to all bilayers, an increased preference for cholesterol-rich ordered domains is seen.

Previous molecular dynamics simulations have shown an increased preference for disordered domains for several transmembrane helical peptides irrespective of helix−lipid mismatch.[33] Confocal microscopy corroborated that the peptides spontaneously partition into the liquid-disordered phase. In fact, the protein LAT that is frequently used as a raft marker was also shown to partition in the cholesterol-poor disordered phase in model membranes. The disruption of lipid packing and the decreased lipid chain order in the liquid ordered domain was shown to dictate the partitioning of these transmembrane peptides. Cav-1 peptides are one of the few membrane peptides that even in the absence of the palmitoyl anchors show an increased preference for the cholesterol-rich ordered phase in model membranes. Although cav-1 is not transmembrane, it also leads to a substantial decrease in the lipid order parameters in DPPC−cholesterol bilayers (Supplementary Figure 1, Supporting Information). In contrast, in DOPC bilayers, lipid chain order parameters are similar in the presence and absence of the peptide. Therefore, the differences in the disorder of lipids upon peptide binding are likely to be a driving force for cav-1 partitioning behavior.

Cav-1 Induced Spontaneous Curvature Is Composition-Dependent. To understand how the interaction of cav-1 peptides with membranes leads to changes in its morphology and whether it is dependent on the composition of the bilayer, we calculated the bilayer pressure profiles and elastic properties such as spontaneous curvature. Lateral pressure profiles have been suggested to play a significant role in many cellular membrane processes,[42] and changes in membrane composition have been shown to affect pressure profiles.[43] The lateral pressure profiles for the two representative systems, peptide bound to DPPC and DPPC−cholesterol mixed bilayers, are shown in Figure 8. In the presence of cholesterol, the lateral

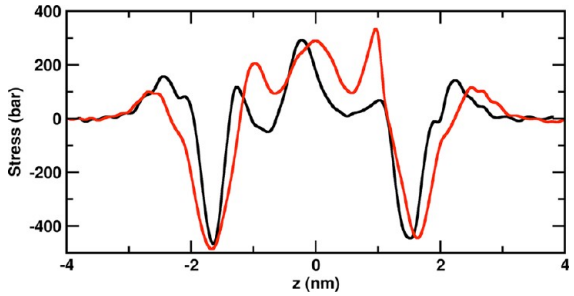

Figure 8. Lateral pressure profiles for DPPC (black) and DPPC−cholesterol (red) bilayers with bound cav-1 peptides.

pressure near the membrane center is increased substantially in comparison with the profile in the absence of cholesterol, consistent with previous findings in peptide-free systems. The pressure profiles were also calculated for a smaller bilayer patch of 4 nm from the peptide. A comparison of the pressure profiles with that of the pure bilayer is shown in Supplementary Figure 2 (Supporting Information). Interestingly, both leaflets of the bilayer are affected, although the peptide is bound to only one leaflet. The largest difference between the pressure profiles of pure and peptide bound membranes was in DPPC−cholesterol. The differences were even larger when we considered only a smaller bilayer patch close to the membrane.

The spontaneous curvature of a lipid bilayer can be calculated from its lateral pressure profiles (see refs 35 and 44) and is also dependent on membrane composition.[45] The values of spontaneous curvature are tabulated in Table 2. The values were calculated for the bilayer patch 4 nm from the

Table 2. Spontaneous Curvature[a]

system	DPPC	DPPC−Chol	POPC	POPC−Chol	DOPC
peptide-bound	−0.2	+0.10	−0.05	−0.19	−0.22
	−0.32	+0.10			
peptide-free	0.00	−0.20	−0.6	−0.3	−0.37
	−0.01	−0.38			
pure bilayer	−0.10	−0.21	−0.15	−0.25	−0.18
	−0.12	−0.28			

[a]The values of the spontaneous curvature calculated from the first moment of the pressure profiles of the five bilayer systems. The first row reports the values at 300 K and the second row at 325 K.

dx.doi.org/10.1021/jp3077886 | J. Phys. Chem. B 2012, 116, 14556−14564

peptide as well as the corresponding peptide-free leaflet. The values of the bilayer systems in the absence of the protein are also reported. All the bilayer systems that have been studied have a negative spontaneous curvature in the absence of peptide. Upon adding cav-1 peptides, a change in the spontaneous curvature is seen. All bilayers except DPPC−cholesterol bilayers have a negative value of spontaneous curvature but with values differing from those of the pure bilayer systems. In DPPC−cholesterol mixed bilayers, a positive spontaneous curvature is calculated at both 300 and 325 K. The spontaneous curvatures calculated for the peptide-free leaflet were also negative, though the values differed from those in pure bilayers. Positive values for the radius of spontaneous curvature reflect an increased preference for positively curved surfaces (such as in micelles, pores), and increasingly negative values correspond to an increasing preference for negatively curved surfaces (inverted phases, stalks). The increased positive pressure in the center of the bilayer that contributes to a positive spontaneous curvature of cholesterol-rich bilayers is consistent with the role of cav-1 in inducing curvature in the first steps during the budding of a vesicle. However, the curvature of the bilayers is very small due to the presence of only a single cav-1 peptide and the role of oligomerization in inducing increased curvature cannot be ruled out.

Molecular Model of cav-1 Induced Morphological Changes in Cholesterol-Rich Lipid Bilayers. The composition-dependent interaction of cav-1 peptides with lipid membranes seen in our simulations can be correlated to its cholesterol-dependent function. An increased preference for cholesterol-rich bilayers is seen for the cav-1 peptides, though no specific interactions were seen with the putative cholesterol binding CRAC residues. The effect of cholesterol on membrane proteins has been attributed to both specific interactions of lipids with amino acid residues or bulk properties of membranes. The increased preference of cav-1 peptides for cholesterol-rich bilayers could arise due to the change in the physical properties of the membrane, such as membrane fluidity and order instead of direct cholesterol binding. Previous experimental studies on cav-1 have also speculated such an indirect effect of cholesterol on the lipid−peptide interactions.[17]

Upon binding to the membrane, cav-1 inserts the least in DPPC−cholesterol mixed bilayers and also has an increased population of "open" conformations. We speculate that the more surface-lying orientations along with the open conformations of cav-1 induces changes in the lipid packing in the leaflet to which it is bound and causes a change in the spontaneous curvature of the membrane. The positive spontaneous curvature it induces in DPPC−cholesterol bilayers could be a first step in inducing large topological changes that result in caveolin formation. Though cav-1 peptides do not have the characteristic "banana shape" of the BAR domain proteins that are also involved in vesicle budding events, it appears that, similar to the BAR domains, the decreased membrane penetration and the increased interhelical angle actually helps to induce membrane curvature. We are currently modeling the full-length cav-1 in order to further understand how the N- and C-terminal residues affect this induced curvature, and in particular the role of oligomerization in bringing about large morphological changes in cholesterol-rich membranes.

CONCLUSIONS

In conclusion, by using coarse-grain molecular dynamics, we have been able to analyze the molecular basis for the cholesterol-dependent partitioning behavior of cav-1 peptides. By comparing the structural, energetic, and elastic properties of several biologically relevant model bilayers, we are able to unravel the molecular forces driving complex phase behavior in biological systems. We find that, even in the absence of any direct cholesterol-binding sites, the partitioning free energy of cav-1 is more favorable for cholesterol-rich bilayers and results in an increased preference for them. Upon binding, a surface-aligned orientation, wherein the peptide is orientated parallel to the bilayer surface, coupled with changes in the pressure profile of the bilayers leads to cholesterol-dependent morphological rearrangements in the membrane. Our results highlight the molecular details of protein−lipid interplay and provide new insights into the effects of cav-1 in tuning the morphology of cholesterol-rich membranes.

ASSOCIATED CONTENT

Supporting Information

Figures showing lipid order parameters, lateral pressure profiles, and population profiles and table showing parameters of the fit of the angle profiles. This material is available free of charge via the Internet at http://pubs.acs.org.

AUTHOR INFORMATION

Corresponding Author

*E-mail: d.sengupta@ncl.res.in.

Notes

The authors declare no competing financial interest.

ACKNOWLEDGMENTS

The author thanks Tsjerk Wassenar for discussions and proofreading, the Ramalingaswami Fellowship (DBT) for funding, and the CoESC, NCL, for computational time.

REFERENCES

(1) Anderson, R. G. *Annu. Rev. Biochem.* **1998**, *67*, 199−225.
(2) Lajoie, P.; Goetz, J. G.; Dennis, J. W.; Nabi, I. R. *J. Cell Biol.* **2009**, *185*, 381−385.
(3) Fielding, C. J.; Fielding, P. E. *Biochim. Biophys. Acta, Biomembr.* **2003**, *1610*, 219−228.
(4) Bonuccelli, G.; Casimiro, M. C.; Sotgia, F.; Wang, C.; Liu, M.; Katiyar, S.; Zhou, J.; Dew, E.; Capozza, F.; Daumer, K.; Minetti, C.; Alpy, F.; Rio, M. C.; Tomasetto, C.; Mercier, I.; et al. *Am. J. Pathol.* **2009**, *174*, 746−761.
(5) Head, B. P.; Peart, J. N.; Panneerselvam, M.; Yokoyama, T.; Pearn, M. L.; Niesman, I. R.; Bonds, J. A.; Schilling, J. M.; Miyanohara, A.; Headrick, J.; Ali, S. S.; Roth, D. M.; Patel, P. M.; Patel, H. H. *PLoS One* **2010**, *5*, e15697.
(6) Bosch, M.; Marí, M.; Herms, A.; Fernandez, A.; Fajardo, A.; Kassan, A.; Giralt, A.; Colell, A.; Balgoma, D.; Barbero, E.; Gonzalez-Moreno, E.; Matias, N.; Tebar, F.; Balsinde, J.; Camps, M.; et al. *Curr. Biol.* **2011**, *21*, 681−686.
(7) Lajoie, P.; Partridge, E. A.; Goetz, J. G.; Pawling, J.; Lagana, A.; Joshi, B.; Dennis, J. W.; Nabi, I. R. *J. Cell Biol.* **2007**, *179*, 341−356.
(8) Couet, J.; Sargiacomo, M.; Lisanti, M. P. *J. Biol. Chem.* **2007**, *272*, 30429−30438.
(9) Li, S.; Song, K. S.; Lisanti, M. P. *J. Biol. Chem.* **2006**, *271*, 568−573.
(10) Schlegel, A.; Lisanti, M. P. *J. Biol. Chem.* **2000**, *275*, 21605−21617.

(11) Dietzen, D. J.; Hastings, W. R.; Lublin, D. M. *J. Biol. Chem.* **1995**, *270*, 6838−6842.
(12) Aoki, S.; Thomas, A.; Decaffmeyer, M.; Brasseur, R.; Epand, R. M. *J. Biol. Chem.* **2010**, *285*, 33371.
(13) Lee, J.; Glover, K. J. *Biochim. Biophys. Acta, Biomembr.* **2012**, *1818*, 1158−1164.
(14) Hoop, C. L.; Sivanandam, V. N.; Kodali, R.; Srnec, M. N.; van der Wel, P. C. A. *Biochemistry* **2012**, *51*, 90−99.
(15) Lan, C. L.; Gallay, J.; Vincent, M.; Neumann, J. M.; de Foresta, B.; Jamin, N. *Eur. Biophys. J.* **2010**, *39*, 307−325.
(16) Aoki, S.; Epand, R. M. *Biochim. Biophys. Acta, Biomembr.* **2012**, *1818*, 12−18.
(17) Epand, R. M.; Sayer, B. G.; Epand, R. F. *J. Mol. Biol.* **2005**, *345*, 339−350.
(18) Uittenbogaard, A.; Smart, E. J. *J. Biol. Chem.* **2000**, *275*, 25595−25599.
(19) Ayton, G. S.; Voth, G. A. *Curr. Opin. Struct. Biol.* **2009**, *19*, 138−144.
(20) Lindahl, E.; Sansom, M. S. P. *Curr. Opin. Struct. Biol.* **2008**, *18*, 425−431.
(21) Leontiadou, H.; Mark, A. E.; Marrink, S. J. *J. Am. Chem. Soc.* **2006**, *128*, 12156−12161.
(22) Sengupta, D.; Leontiadou, H.; Mark, A. E.; Marrink, S. J. *Biochim. Biophys. Acta* **2008**, *1778*, 2308−2317.
(23) Cirac, A. D.; Moiset, G.; Mika, J. T.; Kocer, A.; Salvador, P.; Marrink, S. J.; Poolman, B.; Sengupta, D. *Biophys. J.* **2011**, *100*, 2422−2432.
(24) Herce, H. D.; Garcia, A. E. *Proc. Natl. Acad. Sci. U.S.A.* **2007**, *104*, 20805−20810.
(25) Yesylevskyy, S.; Marrink, S.-J.; Mark, A. E. *Biophys. J.* **2009**, *97*, 40−9.
(26) Fuhrmans, M.; Marrink, S. J. *J. Am. Chem. Soc.* **2012**, *134*, 1543−1552.
(27) Baoukina, S.; Tieleman, D. P. *Biophys. J.* **2010**, *99*, 2134−2142.
(28) Risselada, H. J.; Kutzner, C.; Grubmüller, H. *ChemBioChem* **2011**, *12*, 1049−1055.
(29) Mim, C.; Cui, H.; Gawronski-Salerno1, J. A.; Frost, A.; Lyman, E.; Voth, G. A.; Unger, V. M. *Cell* **2011**, *149*, 137−145.
(30) Blood, P. D.; Voth, G. A. *Proc. Natl. Acad. Sci. U.S.A.* **2006**, *103*, 15068−15072.
(31) Rzepiela, A. J.; Sengupta, D.; Goga, N.; Marrink, S. J. *Faraday Discuss.* **2010**, *144*, 431−443.
(32) Singh, G.; Tieleman, D. P. *J. Chem. Theory Comput.* **2011**, *7*, 2316−2324.
(33) Schaefer, L. V.; de Jong, D. H.; Holt, A.; Rzepiela, A. J.; de Vries, A. H.; Poolman, B.; Killian, J. A.; Marrink, S. J. *Proc. Natl. Acad. Sci. U.S.A.* **2011**, *108*, 1343−1348.
(34) Fuhrmans, M.; Knecht, V.; Marrink, S. J. *J. Am. Chem. Soc.* **2009**, *131*, 9166−9167.
(35) Marrink, S. J.; Risselada, H. J.; Yefimov, S.; Tieleman, D. P.; de Vries, A. H. *J. Phys. Chem. B* **2007**, *11*, 7812−7824.
(36) Monticelli, L.; Kandasamy, S. K.; Periole, X.; Larson, R. G.; Tieleman, D. P.; Marrink, S. J. *J. Chem. Theory Comput.* **2008**, *4*, 819−834.
(37) van Gunsteren, W. F.; Billeter, S. R.; Eising, A. A.; Hünenberger, P. H.; Krüger, P.; Mark, A. E.; Scott, W. R. P.; Tironi, I. G. *Biomolecular Simulation: GROMOS96 Manual and User Guide*; Hochschulverlag AG an der ETH Zuerich: Zurich, Switzerland, 1999.
(38) Berendsen, H. J. C.; Postma, J. P. M.; van Gunsteren, W. F.; Nola, A. D.; Haak, J. R. *J. Chem. Phys.* **1984**, *81*, 3684−3690.
(39) Ollila, O. H. S.; Risselada, H. J.; Louhivuori, M.; Lindahl, E.; Vattulainen, I.; Marrink, S. J. *Phys. Rev. Lett.* **2009**, *102*, 78101-1−78101-4.
(40) Periole, X.; Cavalli, M.; Marrink, S. J.; Ceruso, M. A. *J. Chem. Theory Comput.* **2009**, *5*, 2531−2543.
(41) MacCallum, J. L.; Tieleman, D. P. *Trends Biochem. Sci.* **2011**, *36*, 653−662.
(42) Phillips, R.; Ursell, T.; Wiggins, P.; Sens, P. *Nature* **2009**, *459*, 379−385.
(43) Ollila, O. H. S.; Rog, T.; Karttunen, M.; Vattulainen, I. *J. Struct. Biol.* **2007**, *159*, 311−323.
(44) Hu, M.; de Jong, D. H.; Marrink, S. J.; Deserno, M. *Faraday Discuss.* 2013, 10.1039/C2FD20087B.
(45) Marsh, D. *Chem. Phys. Lipids* **2006**, *144*, 146−159.